SDSS-IV MANGA: RADIAL PROFILES OF SPECIFIC STAR FORMATION RATE IN NEARBY INTERACTING GALAXIES

JOSHUA L. STEFFEN[1], HAI FU[1], AND MANGA TEAM
Draft version June 4, 2020

ABSTRACT

We study the spatial profile of the star formation rate (SFR) in a sample of 202 interacting galaxies within the MaNGA (Mapping Nearby Galaxies at Apache Point Observatory) survey. We find that the specific star formation rate (sSFR) is centrally enhanced in the interacting galaxies by $\sim$0.25 $\pm$ 0.1 but that there is no enhancement or suppression in their disks. We further investigate how these profiles behave as a function of stellar mass, mass ratio, and projected separation. We find that the sSFR profiles are unaffected by the stellar masses of the interacting galaxies; however, they are affected by the mass ratio between the galaxies where the galaxies with the smallest mass ratio feature the largest enhancement. We also find that, in pairs with large mass ratios ($|\Delta\log(M)| = 0.5 - 1.5$), the less massive galaxy of the pair has slightly higher levels of sSFR enhancement, $\sim$0.1 dex. We also find that the level of sSFR enhancement increases with closer projected separations; however, the closest pairs, $\leq$5 kpc, show no signs of sSFR enhancement/suppression. We suspect that these close pairs are merging galaxies which have passed their first pericenter, but the merger induced gas-inflows have yet to reach the centers of the galaxies. We also set a simple model for the future mass growth of the galaxies due to the merger induced star formation. We predict that the paired galaxies in our sample will see a mass growth rate which is XX$\times$ higher than secular mass growth.

Keywords: galaxies: active — galaxies: nuclei — galaxies: interactions

1. INTRODUCTION

In the ΛCDM model, galaxy evolution is a hierarchical process. Over the lifetime of the universe, smaller galaxies have iteratively merged forming more massive galaxies. In fact, cosmological hydrodynamical simulations have shown that repeated merger events may be responsible for as much as $\sim$60% of stellar mass in massive galaxies like M87 (e.g. Rodriguez-Gomez et al. (2016); Pillepich et al. (2018)).

The internal dynamics of these interacting galaxies were first modeled in the seminal work, Toomre & Toomre (1972). Since then, hydrodynamical simulations have expanded upon the N-body simulations of Toomre & Toomre (1972) by modeling gas-dynamics within the galaxies. These simulations show how barred structures develop within the disks of the interacting galaxies due to the tidal torques between them (Barnes & Hernquist 1991). As the bars form, the gases within the galaxy's disk lose angular momentum and get funneled into the centers of the galaxies.

When the gas-inflows impact upon the gases in the nucleus of galaxy a burst of new star formation in triggered (Barnes & Hernquist 1996; Mihos & Hernquist 1996). These gas inflows will also bring metal-poor gases from the disk into the center of the galaxy which can dilute the central metallicity (Rupke et al. 2010; Perez et al. 2011; Scudder et al. 2012). The gas-inflows may also be able to make it into very center of the galaxy and trigger supermassive black hole (SMBH) accretion (Capelo et al. 2017).

Centrally enhanced star formation has also been observed in large spectroscopic surveys including; CfA2 (Barton et al. 2000; Woods et al. 2006), 2dF (Lambas et al. 2003), AEGIS (Lin et al. 2007), SDSS (Ellison et al. 2008), COSMOS (Kartaltepe et al. 2007; Xu et al. 2012), PRIMUS (Wong et al. 2011), and GAMA (Robotham et al. 2014).

This star formation enhancement increases with closer projected separations between the two galaxies (Ellison et al. 2008; Scudder et al. 2012) but has still shown to be detectable at projected separations of 150 kpc (Patton et al. 2013). The level of the star formation enhancement also increases with smaller stellar mass ratios, $|\Delta\log M|$, between the two galaxies (Ellison et al. 2008).

With the recent large integral field spectroscopic (IFS) surveys, interacting galaxies can be studied with unprecedented spatial detail. Where previous spectroscopic surveys were limited to the nucleus of the interacting galaxies, the new IFS surveys will be able to study both the nuclei and the disks of the interacting galaxies.

The IFS surveys, CALIFA[2] and MaNGA[3], have already been used to study the SFR of interacting galaxies in merging galaxies. The SFR was found to be centrally enhanced by a factor of 2–3$\times$ (Barrera-Ballesteros et al. 2015; Pan et al. 2019), which is in agreement with previous single-fiber spectroscopic surveys. These surveys also studied the SFR in the disk of the paired galaxies; however, there is a discrepancy between the results. Barrera-Ballesteros et al. (2015) found a suppression to the SFR of $\sim$0.74$\times$ while Pan et al. (2019) found an enhancement of 1.22–1.58$\times$.

The MaNGA survey has also been used to study the radial profiles of SFR in post merger galaxies, which are the galaxies which have recently coalesced. The post merger galaxies showed a central enhancement to the SFR surface density of 2.5$\times$ and an enhancement in their disks of 1.26$\times$ (Thorp et al. 2019).

In our previous work, Fu et al. (2018), we built a sample of paired galaxies in the MaNGA survey where both components of the pair were contained within field of view of a single IFU. We found that approximately 5.7% of the MaNGA galaxies have a companion galaxies contained with the IFU.

[1] Department of Physics & Astronomy, The University of Iowa, 203 Van Allen Hall, Iowa City, IA 52242

[2] Calar Alto Legacy Integral Field Area
[3] Mapping Nearby Galaxies at Apache Point Observatory

In this work, we will use a version of this sample updated for the recent MaNGA Data Release 16 (DR16) and further supplement this with a sample of companion galaxies identified outside the field of view of the IFUs.

In this work we will expand upon the previous works by studying how the spatial profile of SFR behaves as a function of the stellar mass of the paired galaxy, the mass ratio between the galaxy pairs, and the projected separation between the galaxies. We will also model how the merger-induced star formation will affect the future mass growth of the interacting galaxies.

This paper is organized as follows; in Section 2 we will discuss the detail of the MaNGA survey, in Section 3 we will discuss how we extract emission lines from the MaNGA survey and how we calculate the star formation from them, in Section 4 we discuss the construction of our pair sample, in Section 5 we discuss the construction of our control sample, in Section 6 we build the radial profiles for the pair and control galaxies, in Section 7 we discuss the results of the survey, in Section 8 we discuss our results in the context of other surveys, and in Section 9 we summarize and conclude the work.

2. DATA

MaNGA is an a IFS survey based at Apache Point Observatory (APO) which used the SDSS 2.5 meter telescope along with two dual-channel BOSS spectrographs. MaNGA captures spectra through 17 integral field units (IFUs) with variable numbers of fibers; 19, 37, 61, 91, and 127 fibers covering 12.5″, 17.5″, 22.5″, 27.5″, and 32.5″ on the sky respectively. MaNGA is an optical survey with a spectral coverage of 3600−10,300 Åwith a resolution of R ∼ 2000 and a median spectra coverage of 2.5″FWHM (Bundy et al. 2015).

MaNGA targets galaxies from a subset of 41,154 galaxies with from the NASA-Sloan Atlas (NSA) with a redshift range of $0.01 < z < 0.15$ and a luminosity range of -17.7 $< \mathcal{M}_i <$ -24.0, where $\mathcal{M}_i$ is the rest frame i-band magnitude within the NSA survey's elliptical Petrosian apertures. MaNGA plans to cover 10,000 galaxies with a flat stellar mass distribution at two spatial coverages, 1.5 R_{eff} and 2.5 R_{eff} (where R_{eff} is the radius which contains 50% of the galaxy's total light). In this work we use the data from the internal data release, MPL-8, which covers 6142 unique galaxies.

The MaNGA sample is split into three subsamples; the Primary Sample, Secondary Sample, and Color-Enhanced Sample. The Primary sample contains the galaxies which are covered out to 1.5 R_{eff} and makes up 47% of the survey. The Secondary contains the galaxies which are covered out to 2.5 R_{eff} and makes up 37% of the survey. The Color-Enhanced sample is designed to select rarer galaxy types with a spatial coverage of 2.5 R_{eff} and makes up 16% of the survey.

Because of the survey's flat stellar mass distribution and uniform spatial coverage, these samples have a unique "banana" shaped distribution in redshift and luminosity, see Figure **??**. Because the Secondary and Color-Enhanced samples use a wider spatial coverage than the Primary sample, the Secondary and Color-Enhanced Samples will posses galaxies of higher redshifts than galaxies at the same stellar masses in the Primary sample.

We further use photometric data from the NSA catalog and Simard et al. (2011) (from now on Simard+11). We use the r-band elliptical Petrosian apertures from the NSA catalog and the r-band elliptical Sérsic apertures from Simard+11 to quantify the geometry of the outside-IFU and inside-IFU samples

respectively. We further use the total stellar masses extracted from these apertures to quantify the total stellar masses of the galaxies, the NSA catalog contains their own calculation for stellar mass and we use the stellar mass calculation from Mendel et al. (2014) for the Simard+11 apertures.

3. ANALYSIS

3.1. *Emission Lines*

We use our own IDL based spectral fitting code, SPFIT, to model the spectra from the MaNGA datacubes. SPFIT simultaneously fits emission lines and the stellar continuum with the Levenberg-Marquardt nonlinear least-squares minimization algorithm (Fu et al. 2018). Emission line are parameterized as a Gauss-Hermite series and the stellar continuum is the sum of simple stellar populations (SSPs) convolved with the line-of-sight velocity distribution (LOSVD). The algorithm provides us with measurements of emission line fluxes, equivalent widths, velocities, and velocity dispersions of 19 emission lines and measurements of stellar masses, ages, [Fe/H], and kinematics of the stellar populations.

We use the extinction curve from Cardelli et al. (1989) with updated coefficients from O'Donnell (1994). The extinction in parameterized as $R_V \equiv A_V/E(B-V) = 3.1$ where we estimate the value of the V-band extinction, A_V, by comparing the Hα/Hβ to the expected value of 2.85 for case-B recombination. We apply the extinction correction to all of the extracted emission lines.

3.2. *Star Formation Rates*

We classify galaxies as star forming using both the color-magnitude diagram (CMD) and the BPT diagram (Baldwin et al. 1981). We show the CMD in Figure 1 along with demarcation lines which separate the blue cloud, red sequence, and green valley. We established the demarcation lines by collapsing the CMD to a color histogram for each of the three regions and then varied the slopes between the regions until we found the slopes which best fit the data. These demarcation lines are;

$$NUV - r = 3.1682 - 0.16(M_i + 18) \tag{1}$$

$$NUV - r = 4.7866 - 0.04(M_i + 18) \tag{2}$$

Where NUV−r is the color and M_i is the i-band magnitude.

The BPT diagnostic uses emission line ratios to separate ionization sources, star formation and active galactic nuclei (AGN). The two ionization sources can be separated by either the theoretical maximum starburst line from Kewley et al. (2001) or the analytically fitted line from Kauffmann et al. (2003), given below in Equations 3 and 4 respectively.

$$\log\left(\frac{[\text{O\,III}]\lambda5007}{\text{H}\beta}\right) = \frac{0.61}{\log([\text{N\,II}]\lambda6584/\text{H}\alpha) - 0.47} + 1.19 \tag{3}$$

$$\log\left(\frac{[\text{O\,III}]\lambda5007}{\text{H}\beta}\right) = \frac{0.61}{\log([\text{N\,II}]\lambda6584/\text{H}\alpha) - 0.05} + 1.3 \tag{4}$$

Where [O III]λ5007, Hβ, [N II]λ6584, and Hα are emission line fluxes extracted from the spectra within the inner 2 arcseconds of the galaxies. It has also been shown that hot low mass evolved stars (HOLMES) in retired galaxies can
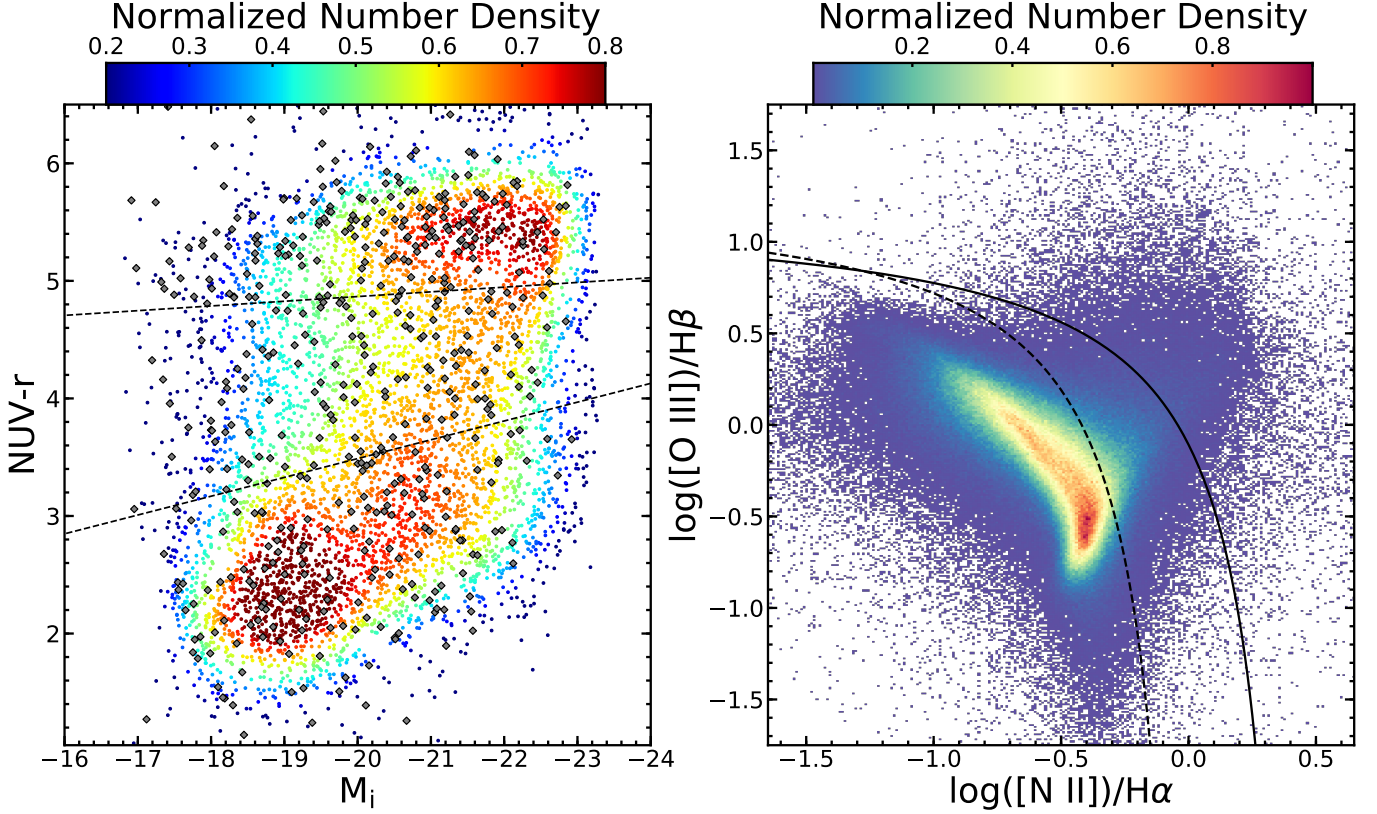
Figure 1. Left: Color-magnitude diagram for MaNGA galaxies (*colored circles*). The color of the symbol reflects the local density around each data point in this color-magnitude plane, as indicated by the color bar on the top. The MaNGA galaxies with close companions are marked with *grey diamonds*. From top to bottom, the dashed lines divide the sample into red sequence, green valley, and blue cloud. The star-forming galaxy sample used in this paper are the galaxies below the lower dividing line. **Right:** The 2-D histogram showing the BPT classification (Baldwin et al. 1981) of individual spaxels within our star-forming control and pair samples. The color of each bin represents the number density of spaxels, normalized to one. The solid black line represents the theoretically determined maximum starburst line of Kewley et al. (2001) and the dashed black line is the analytical Kauffmann et al. (2003) line. This shows the capability of the CMD to select star-forming galaxies as most of the spaxels within the selected galaxies fall beneath the starburst line.

mimic HII regions and AGN on the BPT diagram (Stasińska et al. 2008). We apply an Hα equivalent width (EW) cut of EW(Hα) > 3Åto remove these retired galaxies Cid Fernandes et al. (2011). In this work, we define star forming galaxies as those which are on the blue cloud in the CMD and which is below the Kewley et al. (2001) on the BPT diagram.

We measure the SFR from the Hα luminosity, $L_{H\alpha}$. The Hα luminosity is calculated from the flux of the Hα emission line. We use the SFR formula, Equation 5, from Murphy et al. (2011) which uses a Kroupa IMF, Solar metallicity, a constant SFR at an age of 100 Myr, and Case-B recombination.

$$\frac{\text{SFR}}{M_\odot \, \text{yr}^{-1}} = \frac{L_{H\alpha}}{1.86 \times 10^{41} \, \text{erg s}^{-1}} \qquad (5)$$

We normalize the SFR by the local stellar mass (the stellar mass contained with a given spaxel), calculated from SPFIT, giving us the specific star formation rate (sSFR).

$$sSFR = \frac{SFR}{M^*} \qquad (6)$$

This will allow us to compare the SFR in high mass regions, like the centers of the galaxies, to the SFR lower mass regions, like the disk of the galaxies.

4. PAIR SAMPLE

4.1. *Inside-IFU Sample*

In our previous work, Fu et al. (2018), we showed that ∼5.7% of the MaNGA observations have at least one companion galaxy within the field of view of the IFU. In this work we use a refined pair identification process which is also expanded for the most recent internal data release, MPL-8.

We use SDSS photometric objects to create a catalog of objects within the fields of view of the MaNGA IFUs. The extract their spectra from the MaNGA datacubes through a 1″aperture and fit the spectra with SPFIT. The spectra is then sorted into different categories; "good" galaxy spectra, broad-line AGN, foreground star, foreground/background galaxies, or poor S/N objects. The "good" galaxy spectra are the objects whose spectra is well modeled by SPFIT at the target galaxy's redshift, whether it is the target galaxies itself or a nearby companion galaxy. This means that the companion galaxy can be within ±3000 km s⁻¹ of the MaNGA target. We found 6573 "good" objects, 57 broad-line AGN, 836 foreground stars, 319 foreground/background galaxies, and 1546 objects with poor S/N.

From the 6573 galaxies with good spectra, 404 of the MaNGA IFUs have multiple objects within the IFU and within a relative velocity of $\Delta v < 500$ km s⁻¹. 124 of the galaxies are star forming galaxies (SFGs). Finally, 41 SFGs are covered by Simard+11 and Mendel et al. (2014).

Some of the galaxies in our sample have multiple companions. From the whole set of 404 IFUs, there are 327 pairs, 67 triplets, 7 quadruplets, and 1 quintuplet.

4

We characterize the geometry of the inside-IFU galaxies with the r-band elliptical Sérsic apertures and we characterize the total stellar mass of the galaxies with the stellar masses from Mendel et al. (2014)

4.2. *Outside-IFU Sample*

The second pairs sample is the outside-IFU pairs sample. This sample includes MaNGA galaxies which have companion galaxies found outside the field of view of its IFU. We identify these external pair from the NSA catalog. We select galaxies which are within a projected separation, $r_p < 50$ kpc, and within a relative velocity, $\Delta v < 500$ km s^{-1}.

The NSA catalog contains 641,409 galaxies from which we find 509 galaxies which are paired to MaNGA targets. MaNGA targets which have both an inside-IFU and an outside-IFU pair are left to the inside-IFU sample. After restricting the sample to SFGs, we have 161 MaNGA targets with paired galaxies outside of the IFU.

We use the r-band elliptical Petrosian apertures from the NSA catalog to describe the geometry of the galaxies in the outside-IFU sample. We also use the stellar masses from the NSA catalog for the total stellar mass of the galaxies.

5. CONTROL SAMPLE

We build a sample of isolated control galaxies from the remaining MaNGA galaxies. Selecting the MaNGA galaxies which have no spectroscopic companions within $r_p < 50$ kpc and $\Delta v < 500$ km s^{-1} either inside or outside of the IFU. This gives us a set of 1862 SFGs and 1598 SFGs which are covered by both Simard+11 and Mendel et al. (2014).

The SFR in galaxies has been shown to be dependent on both stellar mass and redshift (Noeske et al. 2007). To account for this we will need to match pairs with similar mass and redshift controls. To do this we build a subset of 20 control galaxies for each paired galaxy.

First we select every control galaxy which is within a stellar mass of 0.1 dex and within in same MaNGA subsample, i.e. the Primary or Secondary sample. Knowing that MaNGA has a tight "banana" shaped distribution in stellar mass and redshift, imposing the stellar mass cut and the MaNGA subsample cut will effectively set a ~0.025 dex redshift cut.

We then downselect the control subset down to 20 controls using a random number generator so that each paired galaxies has the same number of selected controls. In the few cases where a paired galaxy fails to find at least 20 control galaxies, we iteratively expand the stellar mass limits by 0.1 dex until a set of 20 control galaxies can be made. A small set of paired required extra iterations to find 20 controls; 8 paired galaxies need an extra iteration, 1 paired galaxy need two extra iterations, and 1 paired galaxy needed three iterations.

The control galaxies will be treated using both the Simard+11 aperture and Mendel et al. (2014) masses when comparing them to the inside-IFU sample and the NSA apertures and masses when comparing them to the outside-IFU sample.

6. RADIAL PROFILES

As mentioned in Sections 4 and 5 we use the r-band elliptical Petrosian apertures from the NSA catalog and the r-band Sérsic apertures from Simard+11to define the geometries of the galaxies. We calculate the inclination angle, i, of the

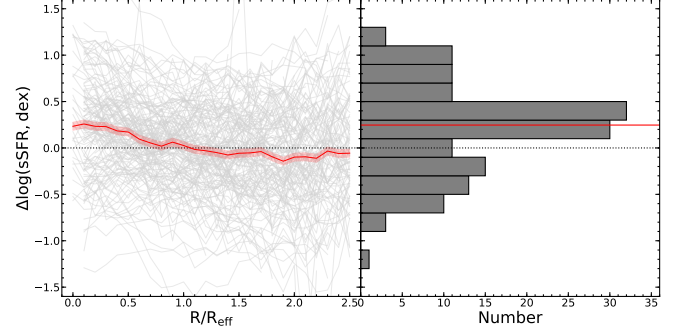**Figure 2. Left:** The individual difference profiles are shown in light grey while the stacked profile for the whole pair sample is shown in red. The highlighted region about the profile is the standard error of the mean of the stacked profile. **Right:** A histogram of the $\delta\log(sSFR)$ within the inner 0.5 R_{eff} of the individual difference profiles. The red line shows the median value of the $\Delta\log(sSFR)$ enhancement, ~0.25 dex.

galaxies using the major-to-minor axis ratios from the elliptical apertures;

$$\cos^2(i) = \frac{(b/a)^2 - q^2}{1 - q^2} \quad (7)$$

The inclination angle is used to deproject the geometries of the galaxies. We use our catalog of photometric objects and the Simard+11 catalog to mask foregournd/background objects. Objects in our photometric catalog are masked out with a 2″ circular aperture and the galaxies from Simard+11 are masked out with a 2.0 R_{eff} elliptical aperture, using the r-band Sérsic apertures from the catalog.

The distance to each of the spaxels from the center of the MaNGA targets is calculated using the 50% half light radius to scale the galaxies. The spaxels are binned into radius increments of 0.1 R_{eff} from 0.0–2.4R_{eff}. Within each radius bin we take the median of the specific star formation rate. The profiles' errors are the standard error of the mean of the data within each radius bin. We create one of these individual averaged radial profiles for every MaNGA galaxy.

We then construct difference profiles between the paired galaxies and the control galaxies. As mentioned in Section 5, a paired galaxy is matched to 20 similar control galaxies. We take the individual averaged profiles of the control galaxies and take the median value of the profiles at each radius bin giving us a "stacked" profile of control galaxies. The error of the profile is the standard error of the mean of the individual profiles. We also take into account the error associated with the random selection of controls using a bootstrapping method to quantify the variation in the values of stacked profile over 1000 iterations. The difference profile is then the difference between a single paired galaxy's profile and the stacked profile in log space (this means that the difference profiles are ratios in linear space). This is done for each of the 202 galaxy pairs.

7. RESULTS

We take each of the individual difference profiles for all of the and take the median value of the sSFR within each radius bin. This gives a single profile which describes the sSFR enhancements for the whole pair sample. We show this profile in the left hand panel of Figure 2. The sSFR is centrally enhanced by ~0.25 dex. The enhancement falls to zero around 1.0R_{eff}. The disks of the paired galaxies feature no enhancement or suppression to the sSFR.
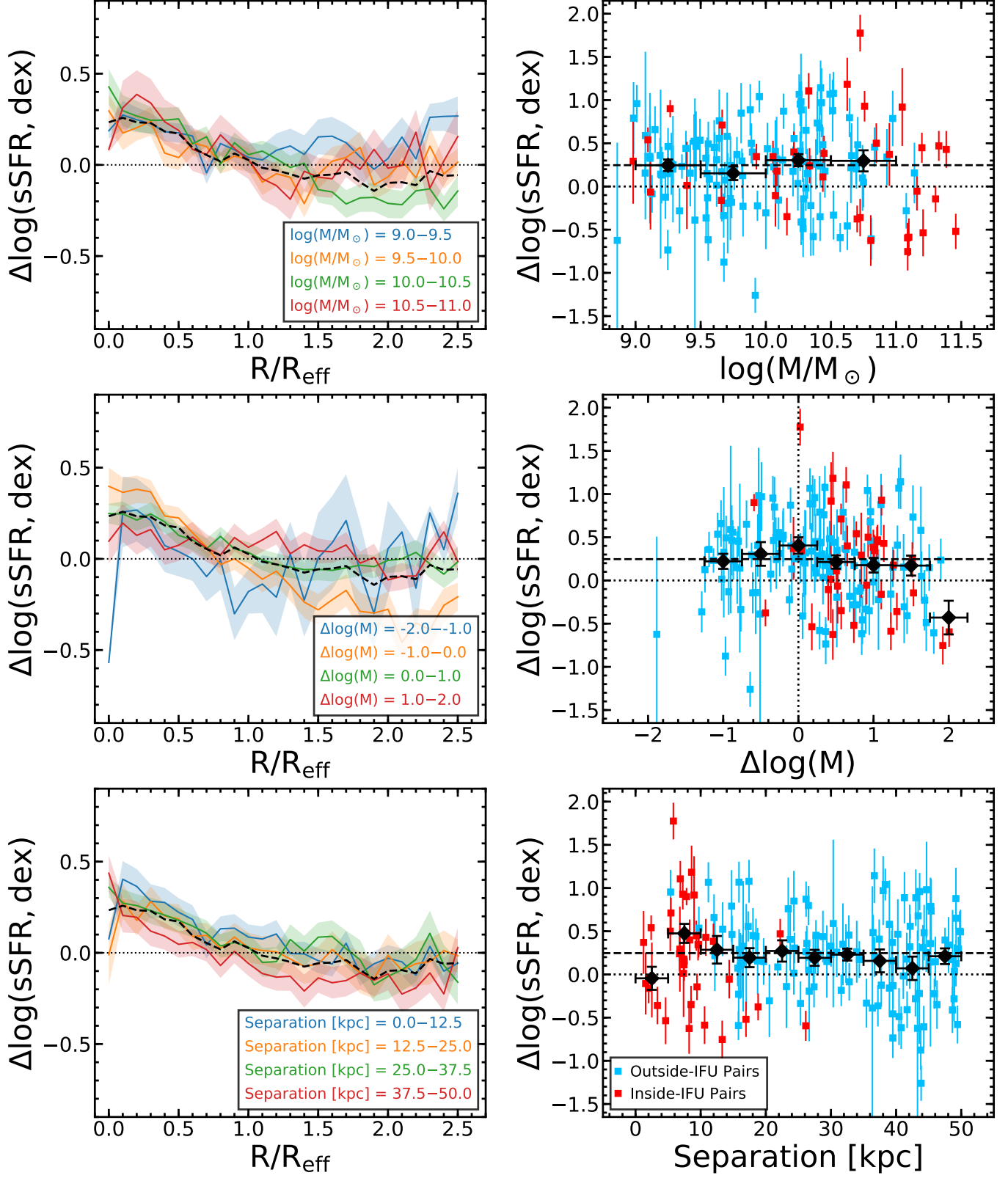
Figure 3. The Δlog(sSFR) split into separate stellar mass bins. The left column gives the stacked difference profiles. The highlighted region about the profiles represents the standard error of the mean of the profile. The black dashed line represents the stacked profile of the full pair sample. The right column gives the nuclear Δlog(sSFR) values. The black squares are the mean values within a stellar mass bin (where the size of the bins are shown the the horizontal error bars). The vertical error bars on the black squares represent the standard deviation within the bin. The horizontal, dashed black lines represent the median central enhancement of the full pair sample. The top row shows the paired galaxies split by total stellar mass, the middle panel shows the paired galaxies split by mass ratio, and the bottom panel shows the paired galaxies split by projected separation.

In the right hand panel of Figure 2 we show a histogram for the Δlog(sSFR) offset in the centers of the paired galaxies. To get this, we extract the values of Δlog(sSFR) in the individual difference profiles within the inner 0.5 R/$R_{\rm eff}$ and take the mean of the values.

In the following sections we will break up the stacked profile into separate bins of total stellar mass, mass ratio, and projected separation.

7.1. Stellar Mass

We show the Δlog(sSFR) profile split by the galaxy's total stellar mass in the top row of Figure 3. The level of the central sSFR enhancement is consistent with the level of enhancement for the full sample. This effect is better seen in the scatter plot of the central Δlog(sSFR) offsets versus stellar mass where there is a flat distribution.

In the disks of the paired galaxies, there is more scatter to the offsets of the profiles. The mass range, log(M/M$_\odot$) = 10.0–10.5, shows stronger suppression of sSFR in their disks while the mass range, log(M/M$_\odot$) = 9.0–9.5, show an enhancement to sSFR in their disks. There is no trend to sSFR enhancement/suppression with the stellar mass so the scatter in the profiles at large separation is likely due to a combination of the smaller sizes within separate mass bins and lower S/N at larger galactocentric radii.

From this we infer that the total stellar mass of a paired galaxy has no effect on the merger induced star formation within the galaxy. Massive galaxies are enhanced to the same degree as low mass galaxies.

7.2. Mass Ratio

While the total stellar mass between the galaxies has no effect on the merger induced star formation, the mass ratio between the paired galaxies does. In the middle row of Figure 3 we see that the sSFR enhancement is strongest in galaxies with mass ratios close to 1:1, δlog(M) = 0.0. These galaxies feature a central enhancement of $\sim$0.4 dex which is 0.15 dex higher than the average central enhancement of the whole sample. This enhancement falls with wider mass ratios and pairs with large differences in stellar mass still feature substantial levels of star formation enhancement, 0.2–0.25 dex at mass ratios of |Δlog(M)| = 1.0.

We also use the mass ratio to explore how the merger induced tidal torques affect paired galaxies with large mass ratios, |Δlog(M)| > 0.5. We use the mass ratio to separate the massive central galaxy from satellite galaxies. A paired galaxy with a positive mass ratio is the more massive galaxy of the pair while a paired galaxy with negative mass ratio is the less massive galaxy. We see that the less massive galaxy of a pair show a higher level of sSFR enhancement, by $\sim$0.1 dex, with respect to the more massive galaxy. This shows us that satellite galaxies are more susceptible to tidal interactions than the central galaxies in the pair system.

7.3. Projected Separation

Finally we look at the level of sSFR enhancement as a function of the projected separation between the two galaxies in the bottom row of Figure 3. The Δlog(sSFR) profiles show a clear gradient with the projected separation where close galaxy pairs show higher levels of sSFR enhancement compared to pairs with wide separations.

This effect can be seen most clearly in the scatter plot of the central Δlog(sSFR) enhancement as a function of projected

separation. The level of the enhancement gradually increases with closer separation from 50 kpc to 10 kpc. Within 10 kpc, the Δlog(sSFR) enhancement jumps to 0.5 dex. Surprisingly, this central enhancement plummets back to zero at the closest separations, $r_p < 5$ kpc. We will discuss the potential causes of the zero enhancement in the centers of the closest galaxies in Section 8.

7.4. Future Mass Growth

The merger induced star formation will increase the mass growth rate of the interacting galaxies. We will use a simple model to estimate the enhanced mass growth rate due to merger induced star formation.

A specific star formation rate is already a representation of the fractional mass growth every year, so the merger induced mass growth is simply;

$$\frac{\Delta M_{merger}}{M_{total}} = \left(sSFR_{pair} - sSFR_{control}\right) * \tau_{dyn} \qquad (8)$$

Where τ_{dyn} is the dynamical timescale of the merger event. For this estimation we use a timescale of 1 Gyr, which is the order of the typical timescale between the passage of the first and second pericenters in hydrodynamical simulations (Boylan-Kolchin et al. 2008).

To get the difference in sSFR between the pairs and controls, we fit a gaussian to the difference profiles split by stellar mass. We then add the modeled difference profile to the stacked control profile in the same mass range in log space. We then take the difference between the profiles in linear space and multiple the difference by the 1 Gyr timescale. This process is shown for a single mass range in Figure 4.

We show the mass growth rate profile for each of the four mass ranges in Figure 5. The mass growth rate is largely restricted to the centers of the galaxies, following the centrally enhanced sSFR. The mass growth rate is strongly dependent on the stellar mass of the paired galaxies.

The fractional mass change is greatest in the less massive galaxies, ΔM$_{merger}$/M$_{total}$ = 0.065, while it is less substantial is the more massive galaxies, ΔM$_{merger}$/M$_{total}$ = 0.015. This is unsurprising as the Δlog(sSFR) profiles were independent of the galaxies' total stellar mass.

Galaxies in the mass range log(M/M$_\odot$) = 9.0–10.0 have a mass growth of $\sim$1.6$\times$ that of secular mass growth and galaxies in the mass range log(M/M$_\odot$) = 10.0–11.0 have a mass growth of $\sim$2.3$\times$ that of secular mass growth. While low mass galaxies may see a more substantial change to their total stellar mass, the more massive galaxies experience higher growth rates.

8. DISCUSSION

The enhancement to the sSFR in the centers of the whole pair sample is consistent with previous galaxy merger studies Ellison et al. (2008); Barrera-Ballesteros et al. (2015); Pan et al. (2019).

Different IFS studies have found different sSFR offsets in the disks of the paired galaxies. Barrera-Ballesteros et al. (2015) found that the sSFR (using EW(Hα) as a proxy) is suppressed in the disks of paired galaxies by $\sim$-0.13 dex. In contrast, Pan et al. (2019) found that the sSFR is enhanced by 0.15 dex. In this work, we see that Δlog(sSFR) is roughly zero but leans towards being suppressed, Δlog(sSFR) = -0.1–0.0 dex.

In previous studies it was noted that the enhancement to the SFR is strongest in galaxy pairs with small mass ratios Elli-
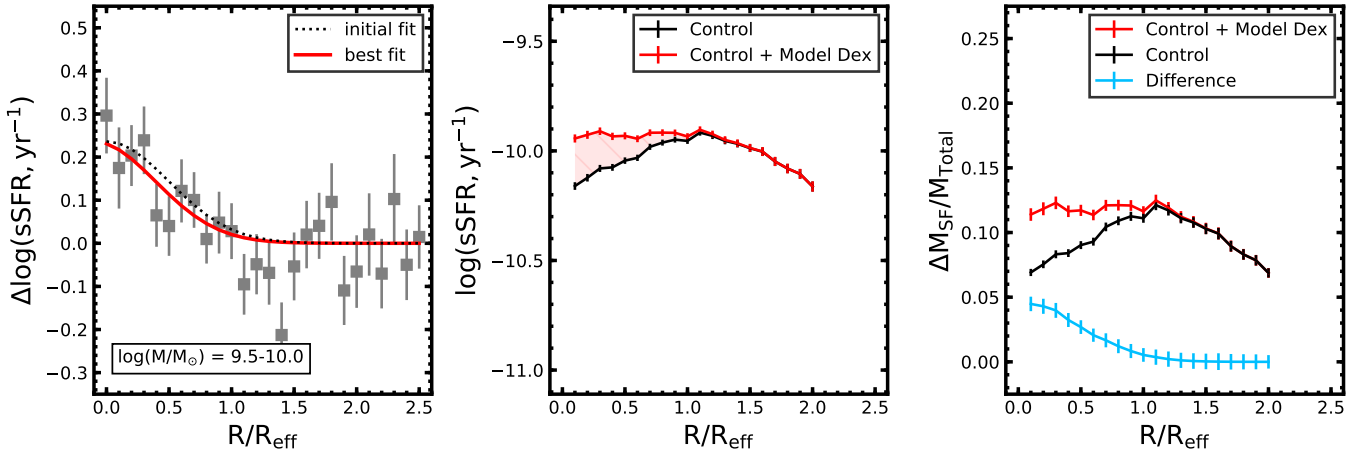
Figure 4. In the Left panel we fit a model gaussian to the $\Delta\log(\mathrm{sSFR})$ profiles. In the Middle panel we plot the $\log(\mathrm{sSFR})$ profile for the stacked profiles of the control galaxies (black). We then add the modeled $\Delta\log(\mathrm{sSFR})$ profile to the control profile (red). The error bars represent the standard error of the mean of the profiles. In the Right panel we show the fractional mass gain due to star formation in the control galaxies (black) and in the paired galaxies (red). The blue profile is the subtraction between the pairs and controls and represents the fractional mass gain due to merger induced star formation. The error bars represent the standard error of the mean of the profiles.
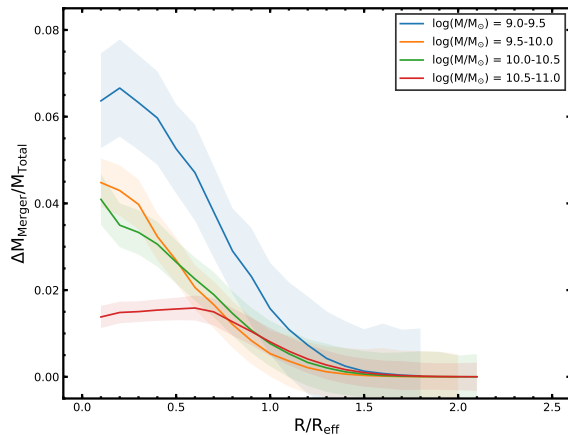

Figure 5. The fractional mass gain due to merger induced star formation over a dynamical timescale, $\tau = 1$ Gyr. The highlighted region represents the propagated standard errors of the mean of the stacked $\log(\mathrm{sSFR})$ profiles.

son et al. (2008). We see the same effect; however, we have also shown that galaxy pairs with large mass ratios still show a substantial level of sSFR enhancement. Further, within these galaxy pairs with wide mass ratios we see that the less massive galaxy in the pair shows higher levels of sSFR enhancement. This implies that satellite galaxies are more affected by interaction induced star formation than the central galaxy.

We saw that the $\Delta\log(\mathrm{sSFR})$ enhancement increases with closer projected separations Ellison et al. (2008); Scudder et al. (2012); Patton et al. (2013). This is unsurprising as nearby galaxy pairs will have just completed a close interaction. This enhancement persists out to wide separations where galaxy pairs separated by 50 kpc still show a substantial enhancement to the sSFR. Patton et al. (2013) showed that the central enhancements to sSFR persists out to 150 kpc.

The closest pairs in our sample, pairs closer than 5 kpc, show no enhancement to the sSFR. This seems odd as one would think that these galaxies should show the strongest enhancements. The first thing to consider is that the sample contains no post-merger galaxies so we will not see the second large burst of star formation when the two galaxies are coalescing. The closest paired galaxies will either be pairs

which are about to go through their first pericenter or galaxies which have just passed their first pericenter. In the galaxies which have passed their first pericenter, we believe that the timescale is still too small for the interaction induced gas inflows to travel from the galaxy's disk to its nucleus. Since the gas inflows haven't impacted the galaxy's nucleus, no enhancements to the sSFR will be seen. Scudder et al. (2012) also found a delay in the burst of merger induced star formation in their hydrodynamical simulations.

9. SUMMARY AND CONCLUSION

We studied a sample of paired, star forming galaxies using the MaNGA IFS survey. We have made a sample of 913 paired galaxies of which 202 are SFGs. We compared the radial profiles of the paired galaxies with 1862 isolated MaNGA SFGs. We found the following;

1. The sSFR is centrally enhanced within the inner $1.0\,R_{\mathrm{eff}}$ by 0.25 ± 0.1 dex.

2. The disks of the paired galaxies, $\mathrm{R}/R_{\mathrm{eff}} = 1.0$–$2.5$, show no signs of either sSFR enhancement or sSFR suppression.

3. The sSFR enhancement in paired galaxies is independent of the total stellar mass of the paired galaxies, Massive galaxies experience the same level of sSFR enhancement as low mass galaxies.

4. The sSFR enhancement in paired galaxies does depend on the ratio between the masses of the paired galaxies. Galaxies with small mass ratios, $|\Delta\log(\mathrm{M})| = 0.0$–$0.5$, see an enhancement to sSFR of 0.4 ± 0.1 dex, which is 0.15 dex higher than the average paired galaxies in the survey. We have also showed that paired galaxies with large mass ratios, $1.0 < |\Delta\log(\mathrm{M})| < 2.0$, still show substantial levels of enhancement to the sSFR, 0.1–0.2 dex.

5. Further, in paired galaxies with large mass ratios, the less massive galaxies experience higher levels of sSFR enhancement than the more massive galaxy in the pair, ~ 0.1 dex.

8

6. The sSFR enhancement increases with closer projected separations where galaxies within 5−10 kpc have their sSFR enhanced by 0.5 ± 0.1 dex. The galaxies within 5 kpc experience no central enhancement to their sSFR. We believe that these galaxies have just passed their first pericenter and the merger induced gas-inflow have yet to reach the centers of these galaxies.

7. The paired galaxies will experience a faster mass growth rate of secular evolution of $1.6-2.3\times$. The growth rate is highest for massive galaxies; however, the the low mass galaxies will see the stellar mass in their center more substantially increased over a 1 Gyr timescale.

REFERENCES

Baldwin, J. A., Phillips, M. M., & Terlevich, R. 1981, PASP, 93, 5
Barnes, J. E., & Hernquist, L. 1996, ApJ, 471, 115
Barnes, J. E., & Hernquist, L. E. 1991, ApJL, 370, L65
Barrera-Ballesteros, J. K., Sánchez, S. F., García-Lorenzo, B., et al. 2015, A&A, 579, A45
Barton, E. J., Geller, M. J., & Kenyon, S. J. 2000, ApJ, 530, 660
Boylan-Kolchin, M., Ma, C.-P., & Quataert, E. 2008, MNRAS, 383, 93
Bundy, K., Bershady, M. A., Law, D. R., et al. 2015, ApJ, 798, 7
Capelo, P. R., Dotti, M., Volonteri, M., et al. 2017, MNRAS, 469, 4437
Cardelli, J. A., Clayton, G. C., & Mathis, J. S. 1989, ApJ, 345, 245
Cid Fernandes, R., Stasińska, G., Mateus, A., & Vale Asari, N. 2011, MNRAS, 413, 1687
Ellison, S. L., Patton, D. R., Simard, L., & McConnachie, A. W. 2008, AJ, 135, 1877
Fu, H., Steffen, J. L., Gross, A. C., et al. 2018, ApJ, 856, 93
Kartaltepe, J. S., Sanders, D. B., Scoville, N. Z., et al. 2007, ApJS, 172, 320
Kauffmann, G., Heckman, T. M., Tremonti, C., et al. 2003, MNRAS, 346, 1055
Kewley, L. J., Dopita, M. A., Sutherland, R. S., Heisler, C. A., & Trevena, J. 2001, ApJ, 556, 121
Lambas, D. G., Tissera, P. B., Alonso, M. S., & Coldwell, G. 2003, MNRAS, 346, 1189
Lin, L., Koo, D. C., Weiner, B. J., et al. 2007, ApJL, 660, L51
Mendel, J. T., Simard, L., Palmer, M., Ellison, S. L., & Patton, D. R. 2014, ApJS, 210, 3
Mihos, J. C., & Hernquist, L. 1996, ApJ, 464, 641
Murphy, E. J., Condon, J. J., Schinnerer, E., et al. 2011, ApJ, 737, 67
Noeske, K. G., Weiner, B. J., Faber, S. M., et al. 2007, ApJL, 660, L43
O'Donnell, J. E. 1994, ApJ, 422, 158
Pan, H.-A., Lin, L., Hsieh, B.-C., et al. 2019, ApJ, 881, 119
Patton, D. R., Torrey, P., Ellison, S. L., Mendel, J. T., & Scudder, J. M. 2013, MNRAS, 433, L59
Perez, J., Michel-Dansac, L., & Tissera, P. B. 2011, MNRAS, 417, 580
Pillepich, A., Nelson, D., Hernquist, L., et al. 2018, MNRAS, 475, 648
Robotham, A. S. G., Driver, S. P., Davies, L. J. M., et al. 2014, MNRAS, 444, 3986
Rodriguez-Gomez, V., Pillepich, A., Sales, L. V., et al. 2016, MNRAS, 458, 2371
Rupke, D. S. N., Kewley, L. J., & Chien, L. H. 2010, ApJ, 723, 1255
Scudder, J. M., Ellison, S. L., Torrey, P., Patton, D. R., & Mendel, J. T. 2012, MNRAS, 426, 549
Simard, L., Mendel, J. T., Patton, D. R., Ellison, S. L., & McConnachie, A. W. 2011, ApJS, 196, 11
Stasińska, G., Vale Asari, N., Cid Fernandes, R., et al. 2008, MNRAS, 391, L29
Thorp, M. D., Ellison, S. L., Simard, L., Sánchez, S. F., & Antonio, B. 2019, MNRAS, 482, L55
Toomre, A., & Toomre, J. 1972, ApJ, 178, 623
Wong, K. C., Blanton, M. R., Burles, S. M., et al. 2011, ApJ, 728, 119
Woods, D. F., Geller, M. J., & Barton, E. J. 2006, AJ, 132, 197
Xu, C. K., Zhao, Y., Scoville, N., et al. 2012, ApJ, 747, 85
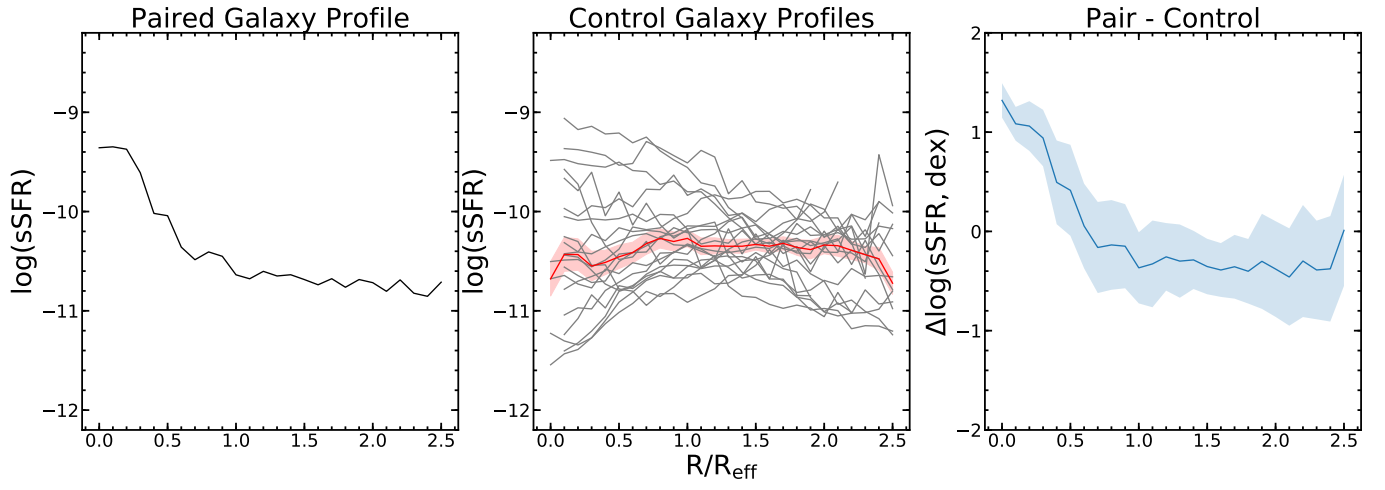
Figure 6. The process for building the tailored control sample. The Left panel shows the paired galaxy's profile for sSFR. The Middle panel shows the profiles for sSFR for the selected 20 control galaxies in gray. The red profile is the median profile of the 20 control galaxies where the highlighted region about the profile is the standard error of the mean. The Right panel shows the difference between pair's profile and the stacked control profile.